ChemComm

COMMUNICATION

View Article Online
View Journal

Cite this: DOI: 10.1039/d5cc03308j

Received 11th June 2025,
Accepted 25th July 2025

DOI: 10.1039/d5cc03308j

rsc.li/chemcomm

Unconventional diastereoselectivity and mechanism of Cp*Co(III)-catalyzed C–H functionalization of asymmetric dienes: a DFT perspective†

Baoping Ling,*[a] Xiaoming Sun,[a] Yuxin Xie,[a] Peng Liu,[a] Wenhui Zhong,[c] Tony D. James[de] and Yuxia Liu*[b]

The Cp*Co(III)-catalyzed C–H functionalization of 2-methyl-substituted dienes and *N*-cyanosuccinimides has been systematically investigated using DFT calculations. Key findings reveal that the unconventional diastereoselectivity for the diene *si*-face insertion over the *re*-face alternative originates from the additional CH…π interaction occurring in the *si*-face pathway. Subsequently, σ-rotation/coordination isomerization accelerates the ligand-to-ligand H-transfer (LLHT) process. Furthermore, an unprecedented "succinimide O-coordination → 3,3-rearrangement → LLHT" mechanism was proposed, in which the succinimide carbonyl group not only relieves the key ∠Co–N^2–C^5 distortion to facilitate 3,3-rearrangement but also ensures a straight N^1···H orbital interaction to promote LLHT. We anticipate that these insights will inspire the development of related C–H functionalization protocols.

Transition-metal catalyzed C–H functionalization has emerged as a powerful synthetic strategy to construct molecular complexes.[1] Despite remarkable progress in this field, in contrast to the two-component strategy,[2] multicomponent C–H activation, especially, three-component sequential C–H addition to two different coupling partners, has been less investigated. Since the pioneering work by Ellman's group,[3] considerable effort has been devoted to various transition metal catalysts, including Co(III),[4] Rh(III),[5] Au(I),[6] Cr/Co bimetal,[7] *etc.*, among which, the Co(III) catalyst has attracted great attention because of its low cost and high earth-abundance.[8]

In the aforementioned context, a series of Cp*Co^{III}-catalyzed three-component C–H addition cascades (Scheme 1) have been developed by the Ellman group.[9–11] As shown in Scheme 1a, the linear diene **S2a** and aldehyde **S3a** are employed as the two coupling partners of the aryl C–H additions, leading to the alcohol **Pa**,[9] while the combination of 2-methyl substituted diene **S2b** and carbonyl **S3b** results in the homoallylic alcohol **Pb** containing acyclic quaternary carbons (Scheme 1b).[10] Intriguingly, the 1,2-disubstituted diene **S2** can combine with the electrophilic cyanating reagent, *N*-cyanosuccinimide (**S3**), through a three-component cyanation reaction, generating the nitrile species **P**, which also bears an acyclic quaternary center (Scheme 1c).[11] These experimental phenomena indicate that three-component C–H activation methodologies by Ellman and co-workers are synthetically meaningful, efficiently introducing a broad array of functionalities to access distinct structural motifs.[12]

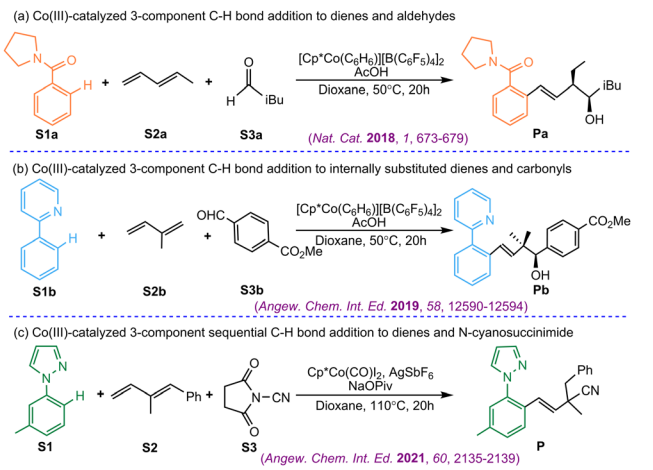

Scheme 1 Co(III)-catalyzed three-component C–H functionalization (a–c) reported by Ellman's group.

[a] School of Chemistry and Chemical Engineering, Qufu Normal University, Qufu 273165, P. R. China. E-mail: xiaoling0523@163.com
[b] Shaanxi Key Laboratory of Chemical Additives for Industry, College of Chemistry and Chemical Engineering, Shaanxi University of Science and Technology, Xi' an 710021, P. R. China. E-mail: liuyuxia2008@163.com
[c] Institute of Intelligent Innovation, Henan Academy of Sciences, Zhengzhou, Henan 451162, P. R. China
[d] Department of Chemistry, University of Bath, Bath, BA2 7AY, UK. E-mail: chstdj@bath.ac.uk
[e] School of Chemistry and Chemical Engineering, Henan Normal University, Xinxiang, 453007, P. R. China

† Electronic supplementary information (ESI) available. See DOI: https://doi.org/10.1039/d5cc03308j

Mechanistically, for this type of reaction, it is commonly accepted that after the (aryl)C–H activation, the terminal C=C insertion of the diene is requisite (Scheme S1, ESI†). However, little information is provided about the diastereoselectivity of the insertion of **S2** (Scheme 1c), which is rarely reported in experimental and theoretical publications.[9–11,13] Moreover, how the (N=)C–N(CCO) bond in **S3** breaks remains unclear, which might imply an unexpected reaction mechanism. Herein, DFT calculations (see the Computational details in the ESI†) were employed to investigate the detailed reaction mechanisms shown in Scheme 1c. In this study, the origin of the diastereoselectivity was unravelled and a unique 3,3-rearrangement/ligand-to-ligand H-transfer (LLHT) mechanism was proposed. We expect that these insights will deepen the understanding of these types of reactions and further inspire the development of related C–H functionalization protocols.

Experimentally, Cp*Co(CO)I_2 (20 mol%), $AgSbF_6$ (40 mol%) and NaOPiv (30 mol%) were employed for three-component C–H functionalization, as shown in Scheme 1c, which can lead to various potential resting states (Fig. S3, ESI†). Calculations confirmed that, among these candidates, [Cp*Co(OPiv)**S1**]$^+$ **Cat0** was thermodynamically the most stable and thus chosen as the energy reference point in the current study. In **Cat0**, [Cp*Co(OPiv)]$^+$ σ-coordinates with one N atom of **S1** and concurrently the –OPiv moiety η^3-interacts with the Co center. As shown in Fig. 1, the reaction is initiated by the aryl C–H activation in **Cat0** to give the Co(III) complex **IM1**, from which, after ligand exchange of **S2** with HOPiv, the C^3=C^4 insertion of **S2** into the Co–C bond will occur.[14] Unexpectedly, the *si*-face insertion *via* **TS6** leading to **IM7** is more favorable kinetically than the *re*-face one *via* **TS3** (17.8 *vs.* 21.5 kcal mol^{-1}).[15] The unconventional diastereoselectivity is clarified by a distortion/interaction analysis (Fig. S7, ESI†). The stronger interaction between the Co-catalyst fragment and the diene fragment is mainly responsible for the stability of **TS6** over **TS3**, and further noncovalent interaction (NCI) analysis (Fig. 1) demonstrates a remarkable C–H…π interaction between the pyrazole ring and one C–H unit of the C^2-attached methyl group in **TS6**. In contrast, little interaction is observed in **TS3**. Therefore, it is believed that the preference of **TS6** over **TS3** in energy mainly originates from the extra C–H…π interaction involved in the former.

Starting from **IM7**, to facilitate the (C^4)H-migration to the C^1 atom (*i.e.*, ligand-to-ligand H transfer), the σ-bond rotation and coordination isomerization (**IM7** → **IM9** → **IM10**) are sequentially followed. And then, the reaction undergoes the LLHT process (see Fig. S8–S11, ESI†). Intriguingly, the calculated results confirmed that such LLHT *via* **TS11** is a concerted step, rather than the experimentally suggested stepwise processes in Scheme S1 (ESI†). Furthermore, the generality of hydride transfer mechanisms of three reactions depicted in Scheme 1 is evaluated (see Fig. S12 and S13, ESI†).

After the LLHT to furnish **IM12**, as displayed in Fig. 2, the *N*-nucleophilic attack of **S3** to the Co center overcomes a barrier of 24.3 kcal mol^{-1} and generates the Co–N σ-species **IM13** (Fig. S14, ESI†), which is exergonic by 14.4 kcal mol^{-1} and considered as the resting state of the reaction. From **IM13**, Ellman's group assumed that **P** is obtained *via* the intermediacy of a Co–N-succinimide species.[11] The computed results show that, upon coordination isomerization of **IM13** to provide the isomer **IM14**, the 1,3-N^1 migration *via* **TS15** gives rise to the Co–N-succinimide intermediate **IM16**. And then the HOPiv-involved

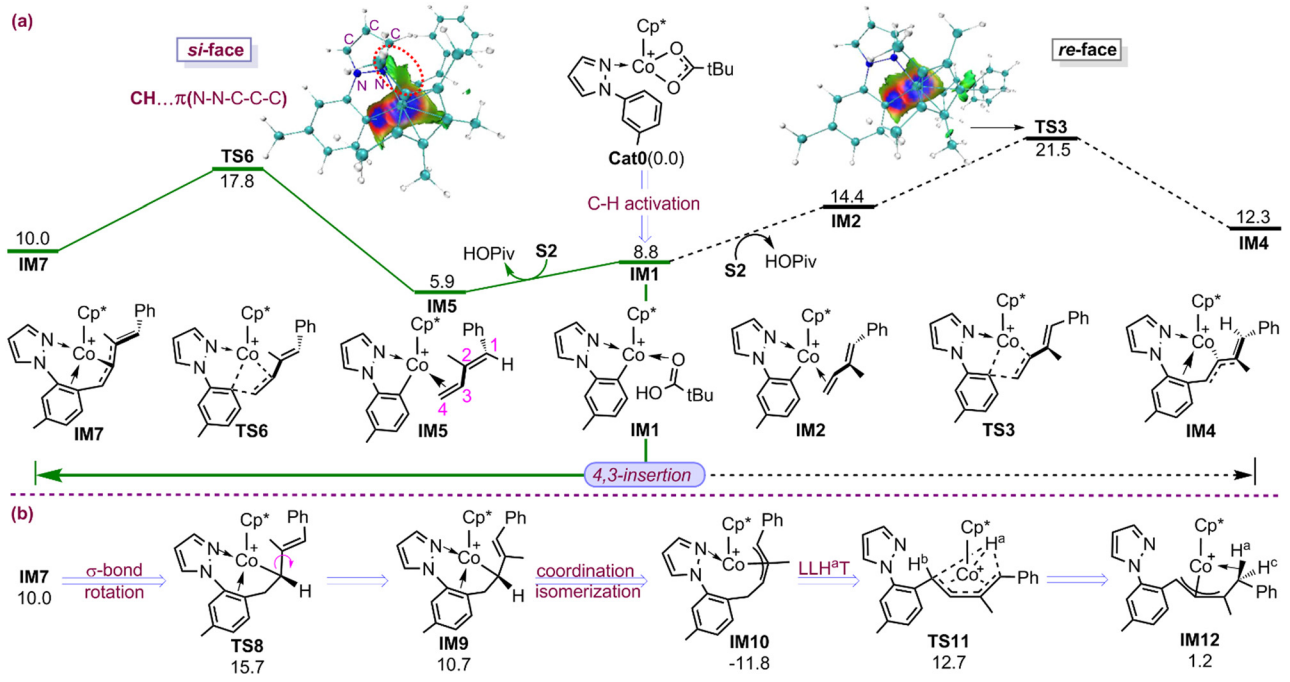

Fig. 1 (a) Free energy profiles for C–H activation/4,3-insertion and NCI analyses for the key 4,3-insertion TSs, **TS3** and **TS6**. (b) The pathway established in this work. Free energies are given in kcal mol^{-1}.

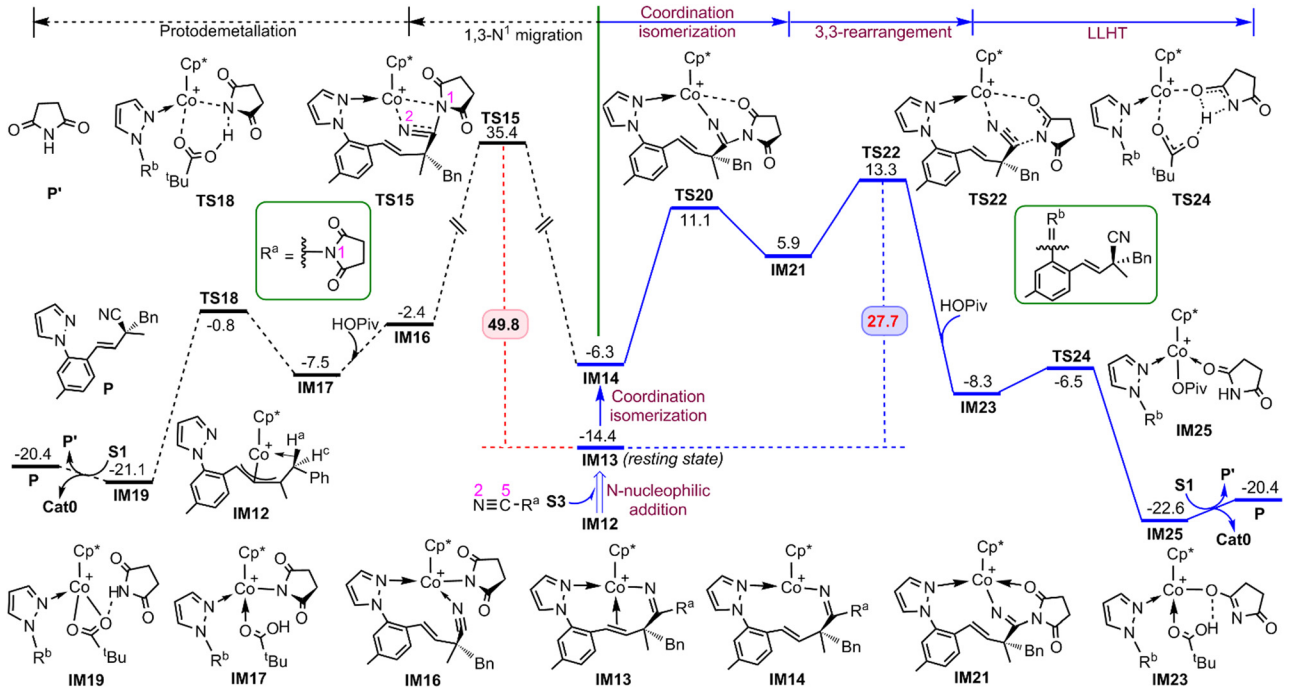

Fig. 2 Free energy profiles leading to **P** from **IM12** according to the experimentally reported route and the newly established one. Free energies are given in kcal mol^{-1}.

protodemetallation occurs *via* **TS18**, leading to **P** and succinimide **P′** and regeneration of **Cat0**.

Unexpectedly, the energy requirement for the 1,3-N^1 migration is calculated to be incredibly high (49.8 kcal mol^{-1}, the difference between **TS15** and **IM13**). The four-membered ring strain in **TS15** is predicted to be the main cause. To circumvent the rigid configuration deformation, we designed a distinctive carbonyl O-coordination induced 3,3-rearrangement/LLHT mechanism, as shown in Fig. 2, featuring the intermediacy of Co–O-succinimide. Beginning with **IM14**, one carbonyl O atom of the *N*-succinimide moiety firstly σ-coordinates with the Co center *via* **TS20**, overcoming an activation barrier of 17.4 kcal mol^{-1}. The resultant isomer **IM21** further undergoes the 3,3-rearrangement *via* **TS22** with an activation barrier of 7.4 kcal mol^{-1} and evolves into adduct **IM23** after HOPiv participation. In the following step, the H(Opiv) migration to the N^1 atom *via* **TS24** provides the LLHT species **IM25**. After the participation of **S1**, the product **P** and succinimide **P′** are released with the regeneration of **Cat0**. From Fig. 2, one can clearly see that the 3,3-rearrangement *via* **TS22** is rate-limiting and involves an overall barrier of 27.7 kcal mol^{-1} (the difference between **TS22** and **IM13**).

In order to reasonably elucidate the newly proposed mechanism, we performed comparative analyses of two transition states for two critical steps involved in Fig. 2: the C^5–N^1 cleavage and H(OPiv)-transfer, and the corresponding computed results are provided in Fig. 3. For the C^5–N^1 cleavage process, **TS22** (3,3-rearrangement TS, 13.3 kcal mol^{-1}) is energetically lower than **TS15** (1,3-N^1 migration TS, 35.4 kcal mol^{-1}), which is closely related to the rigidity of ∠Co–N^2–C^5. As shown in

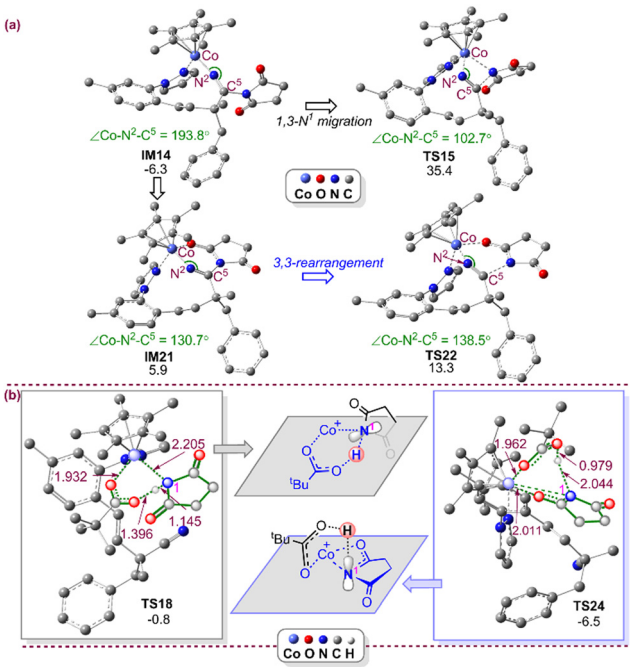

Fig. 3 Geometries with selected structural parameters for key C–N^1 cleavage stationary points, **IM14**, **TS15**, **IM21**, and **TS22** (a) and H(OPiv)-transfer TSs, **TS18** and **TS24** (b). All hydrogens are hidden for clarity. Free energies and bond distances are given in kcal mol^{-1} and Å.

Fig. 3a, ∠Co–N^2–C^5 varies by 91.1° from **IM14** (193.8°) to **TS15** (102.7°). In contrast, it changes by 63.1° from 193.8° in **IM14** to 130.7° in **IM21**, while only by 7.8° from **IM21** to **TS22**

(138.5°). These show that such a large angle distortion in **IM14** → **TS15** brings about significant energy penalty for **TS15**. As far as **IM14** → **TS22** is concerned, on the one hand, the O σ-coordination of the succinimide (**IM14** → **IM21**) remarkably alleviates the rigid ∠Co–N^2–C^5 distortion. And on the other hand, a further small ∠Co–N^2–C^5 change, because of the carbonyl group involvement, makes the resulting 3,3-rearrangement easy (**IM21** → **TS22**). Consequently, **TS22** is energetically preferred over **TS15**, which obviously originates from the crucial role of the succinimide carbonyl group in alleviating the ∠Co–N^2–C^5 rigidity during the reaction.

In the case of the H(OPiv)-transfer TSs (Fig. 3b), **TS24** is found to have lower free energy than **TS18**, −6.5 *vs.* −0.8 kcal mol^{-1}, which is supported by the calculated bond distances. In **TS24**, the O···H (0.979 Å) is much shorter than that in **TS18** (1.396 Å), while the H···N and Co···O (2.044 and 1.962 Å) are longer than 1.145 and 1.932 Å in **TS18**, respectively. Clearly, **TS24** is easier to achieve than **TS18**. This fact might be ascribed to the discrepancy in N···H interaction modes involved. It is shown in Fig. 3b that, in **TS24**, the N^1 site employs its p–π orbital to directly interact with the s orbital of the migrating H atom. Consequently, an excellent head-to-head orbital overlap is presented in the N^1 and migrating H atom. In contrast, structure **TS18** features the interaction between the sp^2–hybrid orbital of the N^1 atom and the s orbital of the migrating H atom, which leads to a small overlap due to the directional deviation of the two orbitals involved. From this perspective, the LLHT *via* **TS24** occurs easier than the protodemetallation *via* **TS18**.

In general, three-component C–H functionalization catalyzed by Cp*Co(III)-catalysts has been investigated using DFT calculations. The *si*-face insertion of 2-methyl-substituted diene **S2** into the Co–C bond is found to be kinetically favoured over the traditional *re*-face one, which can be ascribed to the extra CH···π interaction involved in the former insertion. Subsequently, the σ-bond rotation/LLHT mechanism was proposed to generate the requisite Co-allyl species **IM12**. Upon *N*-nucleophilic attack of **S3** to the Co atom, an unprecedented ''succinimide O σ-coordination → 3,3-rearrangement → LLHT'' mechanism leads to **P**, in which three prominent points are highlighted: (i) the succinimide O σ-coordination effectively alleviates the rigid angle distortion of ∠Co–N^2–C^5; (ii) the participation of the carbonyl group enables the small ∠Co–N^2–C^5 angle deformation and thus contributes remarkably to the stability of the key 3,3-rearrangement TS; and (iii) the strong ''head-to-head'' orbital overlap between the N^1 site and the migrating H atom promotes the LLHT, which is superior to the classical protodemetallation with a directional deviation of the orbitals involved.

This work was supported by the Natural Science Foundation and the Excellent Youth Foundation of Shandong Province (No. ZR2021MB054 and ZR2022YQ16) and the High Performance Computing Center of Qufu Normal University.

Conflicts of interest

There are no conflicts to declare.

Data availability

The data supporting this article have been included as part of the ESI.†

Notes and references

1 For recent reviews on the C–H activation, see: (*a*) Z. Li and Z. Shi, *Acc. Chem. Res.*, 2024, **57**(7), 1057; (*b*) Y. Zhang, J.-J. Zhang, L. Lou, R. Lin, N. Cramer, S.-G. Wang and Z. Chen, *Chem. Soc. Rev.*, 2024, **53**, 3457; (*c*) I. J. S. Fairlamb and J. M. Lynam, *Acc. Chem. Res.*, 2024, **57**, 919; (*d*) B. Garal, D. V. Kumar and B. Sundararaju, *Chem. Commun.*, 2024, **65**, 3354; (*e*) N. Chatani, *Acc. Chem. Res.*, 2023, **56**, 3053.
2 For selected articles on the two-component synthetic strategy: (*a*) G. S. Sontakke, A. K. Chaturvedi, D. Jana and C. M. R. Volla, *Org. Lett.*, 2024, **26**, 4480; (*b*) S. Harada, S. Hirose, M. Takamura, M. Furutani, Y. Hayashi and T. Nemoto, *J. Am. Chem. Soc.*, 2023, **146**, 733; (*c*) J. Meng, H. He, Q. Liu, H. Xu, H. Huang, S.-F. Ni and Z. Li, *Angew. Chem., Int. Ed.*, 2024, **63**, e202315092; (*d*) Y. Naeem, B. T. Matsuo and H. M. L. Davies, *ACS Catal.*, 2024, **14**, 124; (*e*) K. Wu, N. Lam, D. A. Strassfeld, Z. Fan, J. X. Qiao, T. Liu, D. Stamos and J.-Q. Yu, *Angew. Chem., Int. Ed.*, 2024, **63**, e202400509.
3 J. A. Boerth and J. A. Ellman, *Chem. Sci.*, 2016, **7**, 1474.
4 (*a*) P. Prusty and M. Jeganmohan, *Org. Lett.*, 2025, **27**, 3210; (*b*) P. Prusty and M. Jeganmohan, *Chem. Commun.*, 2024, **60**, 10540; (*c*) P. Prusty and M. Jeganmohan, *Chem. Commun.*, 2023, **59**, 7216.
5 R. Li, C.-W. Ju and D. Zhao, *Chem. Commun.*, 2019, **55**, 695.
6 G. Liu, S. Yu, W. Hu and H. Qiu, *Chem. Commun.*, 2019, **55**, 12675.
7 Y. Xiong and G. Zhang, *J. Am. Chem. Soc.*, 2018, **140**(8), 2735.
8 (*a*) D. S. Brandes and J. A. Ellman, *Chem. Soc. Rev.*, 2022, **51**, 6738; (*b*) C. Xu, J. P. Tassone, B. Q. Mercado and J. A. Ellman, *Angew. Chem., Int. Ed.*, 2022, **61**, e202202364; (*c*) J. Yang, D.-W. Ji, X.-C. Hu, X.-T. Min, X. Zhou and Q.-A. Chen, *Chem. Sci.*, 2019, **10**, 9560.
9 J. A. Boerth, S. Maity, S. K. Williams, B. Q. Mercado and J. A. Ellman, *Nat. Catal.*, 2018, **1**, 673.
10 S. Dongbang, Z. Shen and J. A. Ellman, *Angew. Chem., Int. Ed.*, 2019, **58**, 12590.
11 S. Dongbang and J. A. Ellman, *Angew. Chem., Int. Ed.*, 2021, **60**, 2135.
12 For selected articles on three-component C–H activations reported by Ellman and co-workers: (*a*) D. C. Chu, A. J. Zoll and J. A. Ellman, *Org. Lett.*, 2024, **26**, 4803; (*b*) A. J. Zoll, J. C. Molas, B. Q. Mercado and J. A. Ellman, *Angew. Chem., Int. Ed.*, 2023, **62**, e202210822; (*c*) J. P. Tassone, J. Yeo and J. A. Ellman, *Chem. Sci.*, 2022, **13**, 14320; (*d*) D. Chu and J. A. Ellman, *Org. Lett.*, 2022, **24**, 2921; (*e*) D. S. Brandes, A. D. Muma and J. A. Ellman, *Org. Lett.*, 2021, **23**, 9597.
13 X.-K. Zhu, Y.-Q. Zheng and J.-B. Liu, *J. Phys. Chem. A*, 2021, **125**, 5031.
14 For asymmetric branched diene **S2**, all possible modes of alkene insertion into the Co–C bond are examined. Optimized structures for possible transition states are given in Fig. S4 (ESI†).
15 Other competitive C–H activation and diene migratory insertion, such as *syn*-**S2** and **S3** insertion, are calculated and excluded owing to higher energy barriers, see Fig. S5 and S6 (ESI†).

